

e^+e^- Pair Production from 10 GeV to 10 ZeV

Spencer R. Klein

Lawrence Berkeley National Laboratory, Berkeley, CA 94720, USA

Abstract

At very high energies, pair production ($\gamma \rightarrow e^+e^-$) exhibits many interesting features. The momentum transfer from the target is very small, so the reaction probes the macroscopic properties of the target, rather than individual nuclei. Interference between interactions with different atoms reduces the pair production cross section considerably below the Bethe-Heitler values. At very high energies, photonuclear interactions may outnumber pair production.

In contrast, in crystals, the interaction amplitudes may add coherently, greatly increasing the cross sections. Pair production in matter-free magnetic fields is also possible. The highest energy pair production occurs at high energy particle colliders. This article will compare pair production in these very different regimes.

INTRODUCTION

Pair production was first observed by Anderson in 1932, who used the process to discover the positron [1]. Our modern theoretical understanding of pair production stems from work by Bethe and Heitler [2]. At high photon energies, the pair production cross section reaches a constant value [3],

$$\sigma = \frac{7A}{9X_0N_A}, \quad (1)$$

where X_0 is the target radiation length, in units of column density (mass/length², usually g/cm²), A is the atomic mass of the target (usually in g/mole), and $N_A = 6.022 \times 10^{23}$ is Avogadro's number [4]. X_0 is also commonly given in units of length; this length can be multiplied by the density ρ to give X_0 in column density.

Eq. 1 applies at high photon energies, $k > 10$ GeV, when the momentum transfer from the target to the pair is sufficiently small. The atomic electrons screen the nucleus from the incident photon/pair, limiting the effective impact parameter to the Thomas-Fermi radius. In this complete screening limit, the cross section is independent of photon energy. The differential cross section is usually given in terms of $x = E/k$, where E is the electron energy [5]:

$$\frac{d\sigma}{dx} = \frac{A}{X_0N_A} \left[1 - \frac{4}{3}x(1-x) \right]. \quad (2)$$

This lowest order cross section is symmetric in x and $1-x$, the electron and positron energy.

At high energies, two regimes are of interest. Most conversions produce pairs near threshold, with pair mass $M_p \approx 2m$, where m is the electron mass. The momentum transfer required to produce a pair decreases linearly as the photon energy rises. The longitudinal momentum transfer required to produce a lepton pair with energies E and $k-E$ is

$$q_{\parallel} = k - \sqrt{(k-E)^2 - m^2} - \sqrt{E^2 - m^2} \approx \frac{m^2k}{2E(E-k)} \approx \frac{M_p^2}{2k} \quad (3)$$

We take $c = 1$ throughout this review. The approximation in the last two formulae cover are accurate for the vast majority of the cross section, but fail for very asymmetric pairs, where $x \rightarrow 0$ or $x \rightarrow 1$.

As k rises and q_{\parallel} drops, the uncertainty principle requires that the location of the conversion becomes more and more delocalized. The pair production is delocalized over a region

known as the formation length:

$$l_{f0} = \frac{\hbar}{q_{\parallel}} = \frac{2\hbar E(k - E)}{m^2 k} = \frac{2\hbar k}{M_p^2}. \quad (4)$$

The subscript '0' shows that this is for pair conversion in free space; future sections will consider modifications to l_f in dense media. The formation length grows linearly with the photon energy. When the formation length is larger than the typical inter-nuclear separation, interactions with different atoms are no longer independent.

This loss of independence leads to many interesting consequences. In amorphous materials, the pair production cross section decreases as the photon energy rises, invalidating Eqs. 1 and 2. The conversion probability is no longer proportional to the number of target atoms. In moderately thick targets, the conversion probability may even be proportional to the logarithm of the thickness! The reduced cross sections appear in a number of 'real world' situations. For example, they affect electromagnetic showers produced by very high energy cosmic rays.

In crystals, the long formation length allows pair conversion amplitudes from regularly spaced atoms to add coherently. The strong magnetic fields can greatly increase the pair production cross section. This enhancement may be useful in accelerator design.

For very-high-mass pairs, the momentum transfer from the pair is high, and production of these pairs can probe short distance scales. High-mass pairs have been used to test quantum electrodynamics (QED). Neglecting the transverse momentum of the pair (a relatively small effect), the pair mass is

$$M_p^2 = \frac{m^2}{x(1-x)}. \quad (5)$$

Figure 1 shows the pair mass spectrum, $d\sigma/dM_p$. The cross section is strongly peaked near threshold, $x \approx 0.5$ and $M_p \approx 2m$. In this regime, the electron and positron have a small (non-relativistic) relative velocity, and the cross section is enhanced. At even slightly higher masses, the differential velocity is large and the cross section scales as

$$\frac{d\sigma}{dM_p} \propto \frac{1}{M_p^3}. \quad (6)$$

This $1/M_p^3$ dependence continues as long as the momentum transfer to the target is small. When the momentum transfer rises, screening is no longer complete, and the structure of the target becomes significant. In this regime, the cross section decreases faster than $1/M_p^3$.

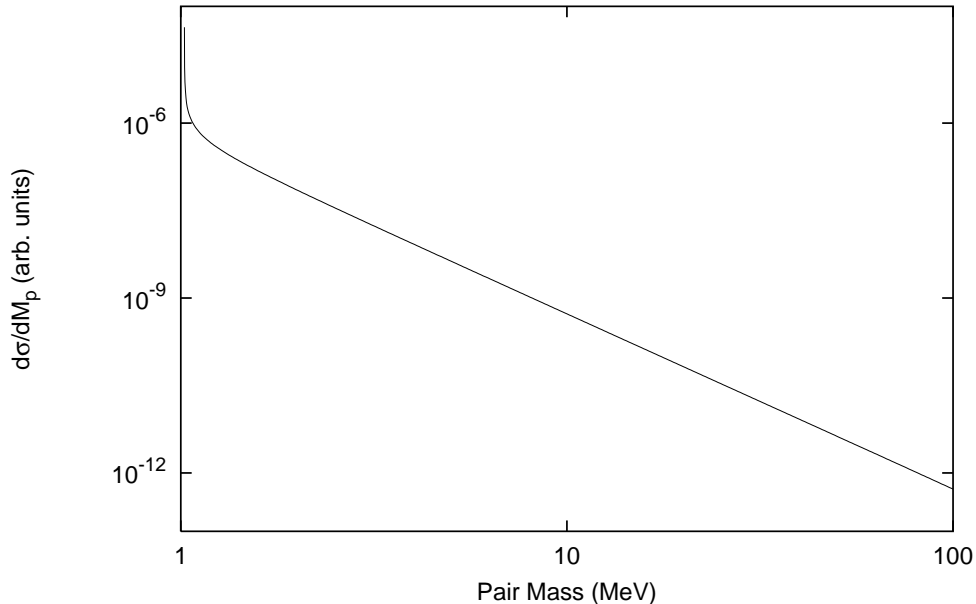


FIG. 1: $d\sigma/dM_p$ for pair production from a 100 GeV photon. The cross section is strongly peaked near threshold. Away from the peak, the cross section scales as $1/M_p^3$. The spectrum is almost independent of the photon energy. For high enough pair masses, the interaction is sensitive to the targets internal structure, and the cross section drops falls off more rapidly.

More recently, QED has been studied at particle colliders, which can reach shorter distance scales. Pair production reactions such as $e^+e^- \rightarrow e^+e^-e^+e^-$ are an important channel for these studies. Another important channel for testing QED has been pair production at heavy ion colliders. Here, the very strong fields are of interest. For gold or lead, the perturbative expansion coupling $Z\alpha \approx 0.6$, and it is not unreasonable to expect significant non-perturbative effects in heavy ion collisions. Here, $\alpha = e^2/\hbar c \approx 1/137$ is the electromagnetic coupling constant, with e the charge on the electron.

High energy electrodynamics in matter has been previously reviewed by Akhiezer and Shulga [6], Baier and Katkov [7], and by Klein [5]. Although it does not address pair production, Ter Mikaelians book [8] has a very interesting, largely classical discussion of high energy bremsstrahlung. Interactions in crystals have been considered by Palazzi [9], Sørensen [10], and by Baier, Katkov and Strakhovenko [11]. Pair production in heavy ion collisions has been recently reviewed by Gerhard Baur and his collaborators [12].

Section 2 of this review considers pair production from isolated atoms. Section 3 will discuss pair production in bulk media. Section 4 will cover production in discrete fields and

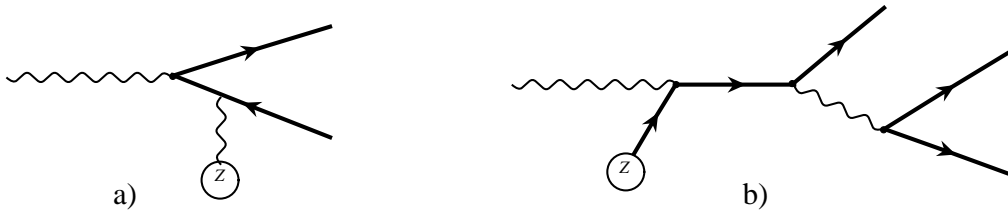


FIG. 2: A schematic diagram of (a) direct pair production on a target with charge Z and (b) pair production via the Compton process. Diagram (a) is usually dominant, and the Compton process (b) is mainly visible via its interference with direct production.

crystals. Section 5 will consider pair production at colliding beam accelerators, and Sec. 6 will draw some conclusions.

PAIR PRODUCTION FROM ISOLATED ATOMS

Pair production from an isolated atom occurs schematically via a two-photon process, as is shown in Fig. 2(a); In the target frame of reference, the incident photon fluctuates to a virtual e^+e^- pair. The pair combines with a virtual photon from the target to form a real e^+e^- pair. In the competing Compton process, Fig. 2(b), the photon is first absorbed by a nucleus or electron, which then emits a virtual photon, which decays to a e^+e^- pair. The Compton amplitude is relatively small, and the process is usually observed via its interference with the direct reaction [2]. This review will focus on the kinematics of pair production, which determines many characteristics of the reaction.

As long as $l_f > a$, where the Thomas-Fermi atomic radius $a = 0.8Z^{-1/3}a_0$ ($a_0 = 5.3$ nm is the Bohr radius) then the nascent pair couples to the target atom as a whole. This is the complete screening limit; at distances larger than a , the electrons screen the nuclear charge. In this limit, the cross section for pair production is independent of k . For heavy ions (heavier than iron), the limit is reached within 1% for $k > 10$ GeV; for lighter ions, higher photon energies are required. For hydrogen, the finite-energy correction is still slightly larger

than 1% for $k = 100$ GeV [13].

For light ions, the radiation length X_0 scales as $1/Z^2$ - the interaction amplitude depends on Z , and the cross section on Z^2 . However, as Z rises, higher order diagrams with multiple photons may be important. The most important (largest) higher order terms account for the fact that the pair is produced in the potential well of the target nucleus; the other terms, due to fluctuations in the incoming photon, are small. Bethe and Maximon calculated the corrections due to the potential by solving exactly the Dirac equation for an electron in a Coulomb field [14]. The solution used Furry wave functions in parabolic coordinates. These radiative corrections reduced the cross section by a constant amount [14, 15],

$$\Delta\sigma(k) = -\frac{28Z^2r_e^2\alpha}{9}f(Z) \quad (7)$$

where $r_e = 2.8$ fm is the classical electron radius and

$$f(Z) = (\alpha Z)^2 \sum_{\nu=1}^{\infty} \frac{1}{\nu(\nu^2 + (\alpha Z)^2)}. \quad (8)$$

For a heavy atom like lead, $f(82) = 0.33$, and the Coulomb correction reduces the cross section about 10%, essentially independent of k .

For the differential cross section, the leading order correction depends only slightly on x . However the next term is large for $x \rightarrow 0$ or $x \rightarrow 1$ [16]. The sign of the second term differs for the two extremes in x , introducing an asymmetry between the electron and positron momentum spectra. These asymmetries have also been studied with perturbation theory; for heavy nuclei, significant asymmetries have been predicted theoretically [17] and observed experimentally [18].

Tsai [13] made detailed calculations of the screening factors and radiative corrections for different materials. He also considered pair conversion on the atomic electrons in the target. The complexities of these calculations can be easily hidden by adjusting X_0 . With this, for $Z > 4$ [4],

$$X_0 = \left(\frac{4\alpha r_e^2 N_A}{A} [Z^2 [\ln(184Z^{-1/3}) - f(Z)] + Z \ln(1194Z^{-2/3})] \right)^{-1}. \quad (9)$$

The first logarithmic term is for nuclear scattering, while the second is for scattering from atomic electrons; $f(Z)$ is the Bethe-Maximon correction. For light nuclei with $Z \leq 4$, the logarithmic terms are inaccurate, and Z -dependent constants are usually used. With this X_0 , Eqs. 1 and 2 remain accurate and easily usable. At 10 GeV, these cross sections agree with the data to within 2% [19].

At very high energies, other channels may contribute to the cross section. For example, the virtual photon in Fig. 2 can be replaced with a virtual Z^0 boson. Although the amplitude for the Z^0 mediated reaction is not large, the interference with the purely electromagnetic process can introduce $\approx 5\%$ asymmetries between the electron and the positron, especially for large M_p [20].

There is a paucity of data on pair production from photons with $k > 10$ GeV. The high-energy frontier has moved to e^+e^- and hadron colliders, as will be discussed in Section 4. There is been considerable data on pair production in crystals, but the effects of the crystal overshadow any subtleties in the individual photon-atom interactions; crystals are discussed in Section .

PAIR PRODUCTION IN MEDIA

As the photon energy rises, the formation length becomes large enough that it encompasses more than one atom. Then, the amplitudes for interacting with multiple atoms must be added, and interference between interactions with different atoms needs to be considered.

Landau and Pomeranchuk considered this problem in 1953 [21, 22]. They used classical electrodynamics to study bremsstrahlung. The emission of photons with momentum \vec{k} and energy $k = |\vec{k}|$, from an electron starting with velocity \vec{v}_1 and ending with velocity \vec{v}_2 into solid angle Ω is [23]

$$\frac{d^2 I}{dk d\Omega} = \frac{Z^2 e^2}{4\pi^2} \left| \frac{\vec{k} \times \vec{v}_1}{\vec{k} \cdot \vec{v}_1 - k} - \frac{\vec{k} \times \vec{v}_2}{\vec{k} \cdot \vec{v}_2 - k} \right|^2. \quad (10)$$

This equation is usually applied to an interaction of an electron with a single atom. Landau and Pomeranchuk realized that, when atoms are close enough together, the interactions cannot be separated. The emission depends only on the initial and final velocities, and is independent of any intermediate state velocities. The scattering due to nearby atoms adds together.

As long as the angle θ_e between \vec{v}_1 and \vec{v}_2 is less than $1/\gamma$, where $\gamma = E/m$ is the Lorentz boost of the electron, then the bremsstrahlung radiation is proportional to $|\vec{v}_1 - \vec{v}_2|^2$ and the radiation from the summed independent (with uncorrelated directions) scattering is the same as if the radiation from each scatterer was added independently. In this case, we define

$\Delta\vec{v} = \vec{v}_1 - \vec{v}_2$, the electron momentum change is $q = \gamma m |\Delta\vec{v}|$, and

$$\frac{d^2I}{dkd\Omega} = \frac{Z^2 e^2 \gamma^4 v^2 \theta_e^2}{\pi^2} \frac{1 + \gamma^4 \theta_e^4}{(1 + \gamma^2 \theta_e^2)^4}. \quad (11)$$

Integrating over the solid angle gives the total emission:

$$\frac{dI}{dk} = \frac{2Z^2 e^2 q^2}{3\pi m^2}. \quad (12)$$

Equation 12 holds as long as the momentum transfer $q < m$. At larger momentum transfers, the radiation is reduced. The cross section for classical bremsstrahlung can be found from Eq. 11.

Landau and Pomeranchuk calculated the radiation from a long electron trajectory that was determined by multiple scattering, with the scattering spread evenly along the path. They determined the interference from radiation from different points on the path. Radiation from nearby points added in-phase, while at larger separations, the phase was random. The phase coherence holds for shorter and shorter distances as the multiple scattering increased. For energetic electrons radiating low energy photons, the reduction in coherence reduces the total emission.

The conditions for reduced emission can be estimated from the multiple scattering in a formation length. When the multiple scattering angle within l_f is larger than $1/\gamma$, then the multiple scattering reduces the coherence, and, with it, the radiation. In a distance l_f , the mean multiple scattering angle is [4]

$$\theta_{MS} = \frac{E_s}{E} \sqrt{\frac{l_f}{X_0}} \quad (13)$$

where $E_s = m\sqrt{4\pi/\alpha} = 21.2$ MeV. An additional multiplicative term, $1 + 0.038 \ln(l_f/X_0)$ is sometimes included to account for the non-Gaussian nature of Coulomb scattering. This non-Gaussian nature is particularly apparent for thin targets, where the number of scatters is small. However, since Eq. 13 is only used for back-of-the-envelope calculations, this multiplicative factor will not be used here.

Neglecting the non-Gaussian scattering tails, and requiring $\theta_{MS} < 1/\gamma$, the emission of photons with energy k from electrons with energy E is suppressed when

$$k < \frac{E^2 E_s^2}{m^4 X_0}. \quad (14)$$

In this limit, the bremsstrahlung spectrum is altered from the Bethe-Heitler prediction $d\sigma/dk \approx 1/k$ to a harder spectrum, $d\sigma/dk \approx 1/\sqrt{k}$!

Although pair production is not a classical process, Landau and Pomeranchuk noted that similar reasoning should apply for it. By using crossing symmetry to relate bremsstrahlung and pair production, they predicted that for photons with very high energies, the pair production cross section scales as

$$\sigma \approx \sqrt{\frac{1}{k}} \quad (15)$$

This is very different from the Bethe-Heitler energy-independent cross section. At high enough energies, photons become penetrating particles.

This cross section can be derived using the uncertainty principle [24] and relying on the proportionality between the pair cross section and formation length. The number of atoms in the formation zone is proportional to l_f . For coherent interactions, the probability scales as the number of atoms squared. The pair conversion amplitudes add in-phase over the formation length, so the interaction probability scales as l_f^2 , and the probability per unit length scales as l_f . Multiple scattering reduces l_f , and with it the cross section.

Multiple scattering changes the electron and positron direction, but not their momenta, reducing their longitudinal velocity. The longitudinal velocity reduction Δv is

$$\frac{\Delta v}{c} = [1 - \cos(\theta_{MS})] \approx \frac{\theta_{MS}^2}{2}. \quad (16)$$

The slowing reduces the longitudinal momentum of the electron and positron. The excess momentum is transferred to the medium during the scattering. Including the multiple scattering from the positron and electron, θ_{MS+} and θ_{MS-} ,

$$q_{||} = \frac{m^2 k}{2E(k-E)} + \frac{E\theta_{MS+}^2}{2} + \frac{(k-E)\theta_{MS-}^2}{2} = \frac{m^2 k}{2E(k-E)} + \frac{E_s^2 l_f k}{2E(k-E)X_0} \quad (17)$$

When $\theta_{MS} > 1/\gamma$ for the electron or positron, the multiple scattering terms dominates. This happens when

$$l_{f0} > \frac{m^2}{E_s^2} X_0, \quad (18)$$

i.e. when

$$k > \frac{m^2 M_p^2 X_0}{2\hbar E_s^2}. \quad (19)$$

In this regime, the multiple scattering angles depend on l_f , which itself depends on θ_{MS} . This leads to a quadratic equation for l_f . When the multiple scattering dominates,

$$\frac{\sigma}{\sigma_{BH}} = \frac{l_f}{l_{f0}} = \sqrt{\frac{kE_{LPM}}{E(k-E)}} \approx \frac{M_p}{m} \sqrt{\frac{E_{LPM}}{k}}. \quad (20)$$

Here, E_{LPM} is a material dependent constant,

$$E_{LPM} = \frac{m^4 X_0}{\hbar E_s^2} \approx 7.7 \text{ TeV/cm} \cdot X_0. \quad (21)$$

For lead, $E_{LPM} = 4.3 \text{ TeV}$. Sometimes E_{LPM} is defined differently, usually differing by a numerical factor (often 2). Since E_{LPM} depends only on X_0 , the pair production cross section may be easily calculated for mixtures.

Pair production is suppressed for photons with $k > E_{LPM}$, *i.e.* in the TeV region and above. In the strong suppression limit ($k \gg E_{LPM}$), the formation length scales as $l_f \approx \sqrt{k}$, and the cross section is suppressed as $l_f/l_{f0} \sim 1/\sqrt{k}$. Suppression is largest for low-mass pairs. This is not surprising; the larger M_p , the shorter l_{f0} (Eq. 4), and the less of an opportunity for multiple scattering to contribute to $q_{||}$.

While the pair production cross section falls at high energies, the photonuclear cross section rises. Photonuclear interactions occur when the photon fluctuates into a quark-antiquark ($q\bar{q}$) pair, which then interacts hadronically with a target nucleus. Very high energy photons may also interact directly with quarks in the nucleus [25].

When the photon energy is high enough, photonuclear interactions may dominate over pair production [26]. Fig. 3 compares the pair production cross section in lead and water (using Migdals suppression, see Sec.) with the photonuclear cross sections. The photonuclear cross sections have not been measured at these energies, but should increase slowly with energy.

For lead, the photonuclear cross section, σ_{had} is about 15 mb when the photon-nucleon center of mass energy, $\sqrt{s_{\gamma N}}$, is less than 100 GeV, and $15(\sqrt{s_{\gamma N}/100\text{GeV}})^{0.2}$ mb at higher energies. For water, $\sigma_{had} = 1.9 \text{ mb}$ for $\sqrt{s_{\gamma N}} < 100 \text{ GeV}$, and $1.9(\sqrt{s_{\gamma N}/100\text{GeV}})^{0.2}$ mb at higher energies. These parameterizations roughly follow Fig. 5 of Ref. [25]; the oxygen cross section is scaled from carbon as the nuclear cross section, $A^{2/3}$, and the water cross section is the sum of its constituent cross sections. Any estimate in this energy range requires a large extrapolation, so there is considerable uncertainty. The energy-dependence in Ref. [25] is reasonably conservative.

There are also significant uncertainties in the pair production cross section. The cross section calculations may fail when the suppression becomes very large (order of $\alpha \approx 1/137$). When LPM suppression is very large, higher-order reactions such as $\gamma A \rightarrow e^+e^-\gamma A$ are more important. With their larger inherent $q_{||}$, these reactions are less affected by multiple scattering.

With these caveats, for both materials the photonuclear cross sections are larger than the pair production cross sections for $k > 4 \times 10^{19}$ eV. The crossover energy is similar for both materials. For lighter materials, σ_{had}/σ_{BH} is larger, while for heavier materials, LPM suppression is larger. The two effects largely cancel out.

Even with the uncertainties, the trend is clear: at very high energies, photonuclear interactions become more important, and may even dominate over pair production. Even at a few 10^{17} eV, electromagnetic showers may develop significant hadronic components, complicating their identification.

Production of $\mu^+\mu^-$ and $\tau^+\tau^-$ pairs, $\gamma \rightarrow l^+l^-$ is reduced by a factor $(m/m_l)^2$, where m_l is the lepton mass. So, neither process is very important here. Of course, in some parts of phase space (such as for high mass pairs), the suppression is smaller.

One other suppression mechanism should be mentioned: bremsstrahlung can also suppress pair production [5, 27]. A produced leptons can emit a bremsstrahlung photon and lose momentum. When the bremsstrahlung occurs in the pair production formation zone, the combined reaction is a single, higher-order process. the bremsstrahlung will increase $q_{||}$, decreasing l_f , and with it, the pair production cross section.

In a crude model, the kinematics changes when $l_f > X_0$. This only happens at very high energies, when the LPM effect is already important. Including LPM suppression, $l_f > X_0$ when $k > E_s^2 X_0/\hbar$, or, for lead, $k > 4 \times 10^{19}$ eV. This is only approximate; while bremsstrahlung suppresses pair production, the reverse is also true: pair production suppresses bremsstrahlung. The suppression of one reaction reduces its impact on the other reaction [26] and a combined calculation is needed to properly understand pair production and bremsstrahlung in this energy regime.

The energies required to study LPM suppression of pair production are well beyond the reach of existing accelerators. However, LPM suppression is important to studies of very high energy cosmic rays (including neutrinos). When high energy cosmic rays hit the atmosphere, they interact, forming air showers which develop into billions of lower energy

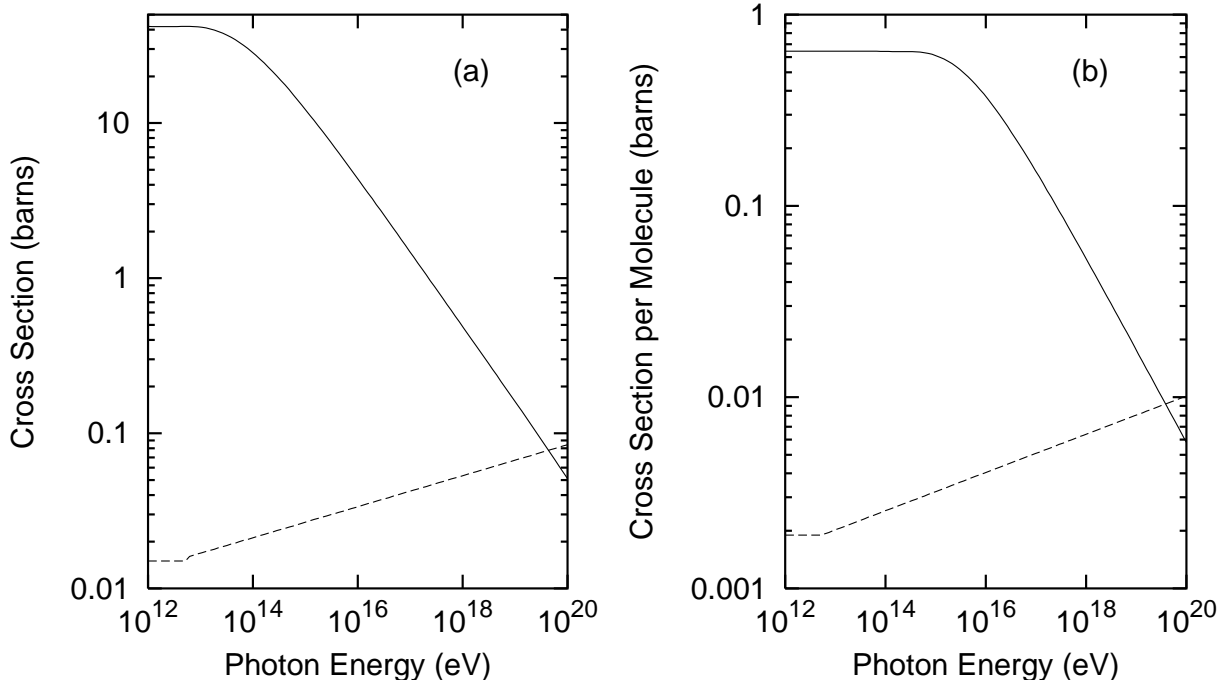


FIG. 3: Cross sections for $\gamma \rightarrow e^+e^-$ (solid line) compared with the cross section for photonuclear interactions (dotted line) in (a) lead and (b) water. Caveats for the curves are discussed in the text.

particles. Cosmic rays with energies up to 3×10^{20} eV have been observed [28]. If the incident particles are photons (unlikely, as discussed in Section), then LPM suppression reduces the cross sections and thereby lengthens the shower, increasing the amount of energy that reaches the ground. Proton induced showers are much less affected, but still have an electromagnetic component that is subject to the LPM effect. However, the suppression is only relevant for the highest energy showers [29]. As will be discussed in Section , cosmic ray showers have been used to study the LPM effect.

Very high energy cosmic ray ν_e , ν_μ and ν_τ may be visible at next generation neutrino detectors, like IceCube [30]. Neutrino interactions produce high energy leptons along with hadronic showers from the struck nucleus. ν_e showers are most affected by the LPM effect, because of the very high energy electron. However, electrons from τ decay and the electromagnetic component of the hadronic shower may also be affected by LPM suppression.

Thin Targets and Surface Production

In very thin targets, the formation length may be larger than the target thickness T . When this occurs, the target interacts as a single unit. Including LPM suppression, $l_f > T$ when

$$k > \frac{2mT}{\hbar} \approx 2.5 \text{ TeV} \cdot T(\mu\text{m}). \quad (22)$$

When $l_f > T$, LPM suppression may be less than in a very thick target.

For very thin targets, the multiple scattering in the target is negligible, and the Bethe-Maximon cross section is retained, independent of k . The Bethe-Maximon cross section applies when the q_{\parallel} from the multiple scattering (the second term in Eq. 17, with T replacing l_f) is less than that due to the pair production (the first term in Eq. 17). This occurs for target thicknesses $T < (m/E_S)^2 X_0$.

For slightly thicker targets, $(m^2/E_S^2)X_0 < T < l_f$, the conversion probability depends on the total scattering in the target. This regime has been studied only for bremsstrahlung [31]. Assuming that the behavior is the same, for $k \gg E_{LPM}$, the conversion probability scales as $\ln(E_S^2 T/m^2 X_0)$ - as the logarithm of the target thickness!

When $T > l_f$, the target no longer acts as a single unit. However, there is an increased probability of interactions within l_f of the target surface. The additional interactions are known as transition pair creation, analogous to transition radiation. The plasma frequency of the medium, ω_p plays a key role. For solids, $\hbar\omega_p$ is 30-80 eV, so about $\hbar\omega_p \approx 10^{-4}m$. Taking $a = \hbar\omega_p/m$, [32]

$$P = \frac{\alpha}{2\pi} \left(\frac{8a^2}{35} + \frac{256a^3}{256} \right), \quad (23)$$

independent of the incident photon energy. In a typical solid $a \approx 10^{-4}$ and $P(a) \approx 10^{-10}$, so this effect is generally negligible.

At higher energies, there are additional surface effects due to multiple scattering. A new type of transition radiation occurs as the electrons electromagnetic fields rearrange themselves to account for the multiple scattering in the medium. Ternovskii calculated the differential probabilities for bremsstrahlung and pair production in plates of moderate thicknesses [33]. For plates that are at least $T_0 = \alpha X_0/2\pi\xi$, ($1 \leq \xi \leq 2$ rises slowly with k to account for the increasing shower length), the differential probability for pair production

is

$$\frac{dN}{dk} = \frac{\alpha}{2\pi k} \left(1 + [x^2 + (1-x)^2] \ln\left(\frac{T}{T_0}\right) \right). \quad (24)$$

The scaling with target thickness T is far from linear! This equation only holds for relatively thin targets. For thick targets, surface transitions are treated as an add-on to production in the bulk of the target. Ternovskii gave formulae for surface transitions which add-on to Migdals calculation of bulk transitions discussed in the next section.

Migdal Formulation for Pair Production

In 1956, Migdal published the first accurate calculation of suppression of pair production [34]. He focused on bremsstrahlung, but also provided formulae for pair production using crossing symmetry. He represented the transition probabilities with a density matrix, and then averaged the density matrix over the possible positions of the scattering centers. This led to a Boltzman transport equation for the radiation. He solved this with the Fokker-Planck technique.

This approach used the quantum mechanical matrix elements, with proper account of electron spin, photon polarization and nuclear recoil. The scattering was realistically (randomly) distributed in space (albeit with a Gaussian distribution for angles).

Migdal expressed his results in terms of two functions $G(\bar{s})$ and $\phi(\bar{s})$, where \bar{s} depends on the photon and electron energies, and on the total radiation (Migdal used s to discuss bremsstrahlung, and \bar{s} for pair production; the two variables are closely related):

$$\bar{s} = \sqrt{\left(\frac{E_{LPM}k}{8E(k-E)\xi(\bar{s})}\right)} \quad (25)$$

The factor $\xi(\bar{s})$ increases from 1 to 2 as the pair production moves from no suppression ($\bar{s} > 1$, the Bethe-Heitler limit) to strong suppression ($\bar{s} \ll 1$):

$$\begin{aligned} \xi(\bar{s}) &= 1 && (\bar{s} \geq 1) \\ \xi(\bar{s}) &= 1 + \ln(s)/\ln(s_1) && (s_1 < \bar{s} < 1) \\ \xi(\bar{s}) &= 2 && (\bar{s} < s_1) \end{aligned} \quad (26)$$

with $s_1 = Z^{2/3}/184^2$. Migdal did not discuss mixtures of materials. However, the radiation is dominated by high- Z materials, it is not too far wrong to take the Z of the heaviest

atom in a mixture. Alternately, one could, following the approach used for X_0 [4], take a weighted average, weighting the different materials by their abundance times Z^2 .

The equations for \bar{s} and ξ can be solved recursively. However, $\xi(\bar{s})$ varies very slowly, and Stanev and collaborators found an approach that avoids the recursion [35]. They defined \bar{s}' following Eq. 25, with $\xi = 1$. Then,

$$\begin{aligned}\xi(\bar{s}') &= 1 & (\bar{s}' \geq 1) \\ \xi(\bar{s}') &= 1 + h - \frac{0.08(1-h)[1-(1-h)^2]}{\sqrt{2s_1}} & (\sqrt{2s_1} < \bar{s}' < 1) \\ \xi(\bar{s}') &= 2 & (\bar{s}' < \sqrt{2s_1})\end{aligned}\tag{27}$$

where $h = \ln(\bar{s}') / \ln(\sqrt{2s_1})$.

The differential cross section for pair production is

$$\frac{d\sigma}{dE} = \frac{A\xi(\bar{s})}{3X_0N_Ak} \left(G(\bar{s}) + 2 \left[\frac{E^2 + (k-E)^2}{k^2} \right] \phi(\bar{s}) \right).\tag{28}$$

Migdal gave infinite series for $\phi(\bar{s})$ and $G(\bar{s})$. However, they may also be represented as polynomials [35]:

$$\phi(\bar{s}) = 1 - \exp \left[-6\bar{s}[1 + (3 - \pi)\bar{s}] + \bar{s}^3 / (0.623 + 0.79\bar{s} + 0.658\bar{s}^2) \right]\tag{29}$$

and

$$\psi(\bar{s}) = 1 - \exp[-4\bar{s} - 8\bar{s}^2 / (1 + 3.96\bar{s} + 4.97\bar{s}^2 - 0.05\bar{s}^3 + 7.5\bar{s}^4)]\tag{30}$$

with $G(\bar{s}) = 3\psi(\bar{s}) - 2\phi(\bar{s})$. Figure 4 shows these functions.

The limit $\bar{s} \rightarrow \infty$, $\xi(\bar{s}) = 1$ corresponds to low photon energies, where $\phi(\bar{s}) = G(\bar{s}) = 1$ and the Bethe-Heitler cross section holds.

The limit $\bar{s} \rightarrow 0$, $\xi(\bar{s}) = 2$ corresponds to strong suppression. Then, $\phi(\bar{s}) = 6\bar{s}$, $G(\bar{s}) = 12\pi\bar{s}^2$ and the cross section is

$$\frac{d\sigma}{dE} = \frac{4A}{3X_0N_Ak} \left(\frac{E^2 + (k-E)^2}{k^2} \right) \phi(\bar{s}).\tag{31}$$

Figure 5 shows the pair production cross sections vs. E/k in lead for different photon energies. At very high energies, most conversions produce asymmetric pairs.

Figure 6 gives the suppression (compared to Bethe-Heitler) as a function of pair mass in lead for photons with energies from 44 TeV to 440 PeV. The suppression is largest for

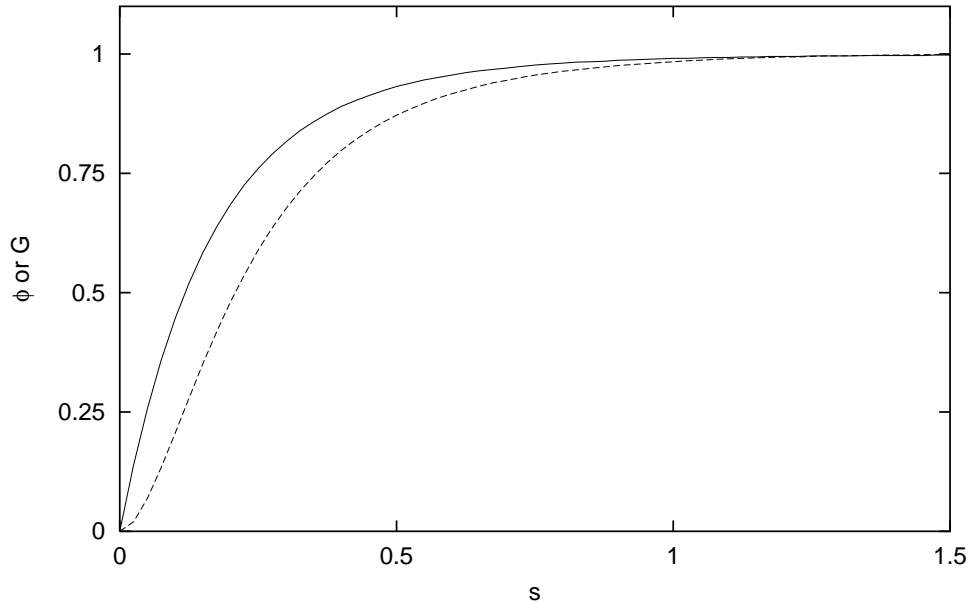


FIG. 4: Migdals $G(\bar{s})$ (dashed line) and $\phi(\bar{s})$ (solid line).

small M_p . The Bethe-Heitler $d\sigma/dM_p$ shape is independent of k , so the cross section is the product of this suppression factor with the cross section from Fig. 1. The bulk of the cross section is near threshold, so the overall suppression is dominated by the measurement around $2m \approx 1.12$ MeV. This calculation neglects the lepton transverse momenta, but most of the consequent inaccuracy should cancel for the suppression. Very roughly, in the strong suppression limit, for $M_p \gg 2m$ the cross section scales as $d\sigma/dM_p \approx 1/M_p^2$.

When the cross section suppression is large, the penetration depth of electromagnetic showers increases significantly. Not only is the total cross section reduced, but either the electron or positron takes most of the energy.

Newer Calculations

Several recent papers have presented more sophisticated calculations of LPM suppression. These calculations consider targets as an integral whole, and therefore naturally handle finite target thicknesses. However, many authors considered only bremsstrahlung. Often, too little information is given for an outsider to easily apply the calculations to pair production. They also do not consider mixtures of atoms with different Z . Blankenbecler and Drell used an eikonal approach to study bremsstrahlung in finite targets [36].

Zakharov used a light cone path integral approach to study bremsstrahlung. He used a

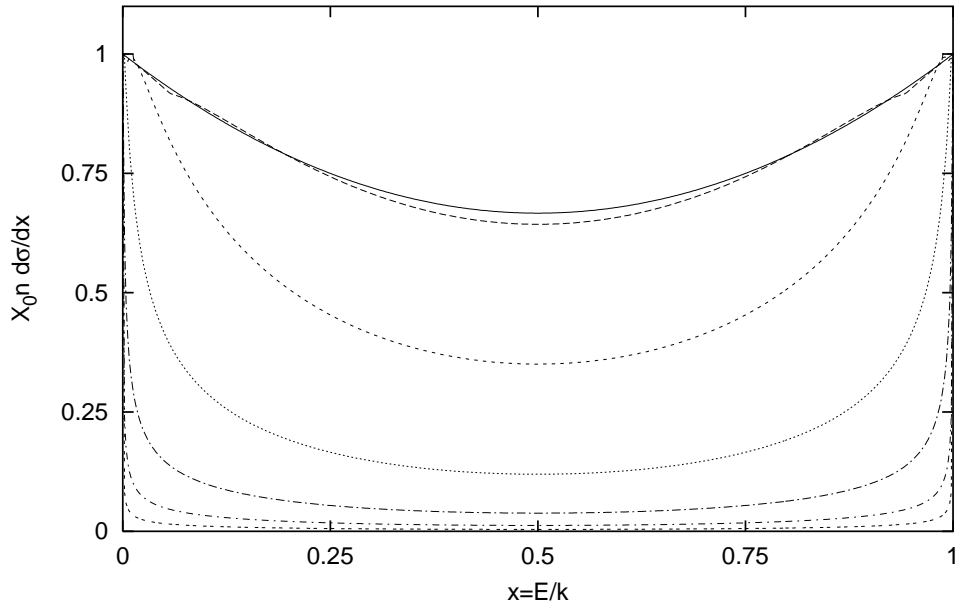


FIG. 5: Differential cross section for pair production, Eq. 28, in a lead target, for different photon energies. Cross sections are shown for photons with $k = 1$ TeV (top), 10 TeV, 100 TeV, 1 PeV, 10 PeV, 100 PeV and 1 EeV (bottom). Here, n is the number of atoms per unit volume. When $E(k - E) \approx 1.2kE_{LPM}$, the product $\phi(\bar{s})\xi(\bar{s})$ rises slightly above 1 and the conversion probability for high energy photons is slightly larger than at smaller k . These curves can be used for other materials by scaling k by $E_{LPM}(\text{lead})/E_{LPM}$; the bottom curve also applies for 3.2 EeV photons in iron ($E_{LPM} = 13.6$ TeV).

transverse Green's function to represent e^+e^- pair scattering from the atom and used it to solve the Schroedingers equation. He used an imaginary potential for the Greens function, proportional to the cross section for an e^+e^- pair to scatter from the atom.

In the strong suppression limit, the scatterer is a dipole with length ρ ; the scattering cross section $\sigma(\rho) = C(\rho)\rho^2$ where $C(\rho)$ varies slowly with ρ [37]. With a constant $C(\rho)$, this is Gaussian scattering. For an infinitely thick target, the results are almost identical to Migdals. With a slowly varying $C(\rho)$ to model Coulomb scattering, the Zakharov cross section has more energy dependence than Migdals $\xi(\bar{s})$. At higher energies, Zakharov should find slightly lower cross sections than Migdal.

For regimes with moderate suppression, Zakharov adopted a more accurate Coulomb potential than a dipole, with separate potentials for the nucleus and it's electrons. This separation is important for low- Z atoms where the electrons play a significant role [38].

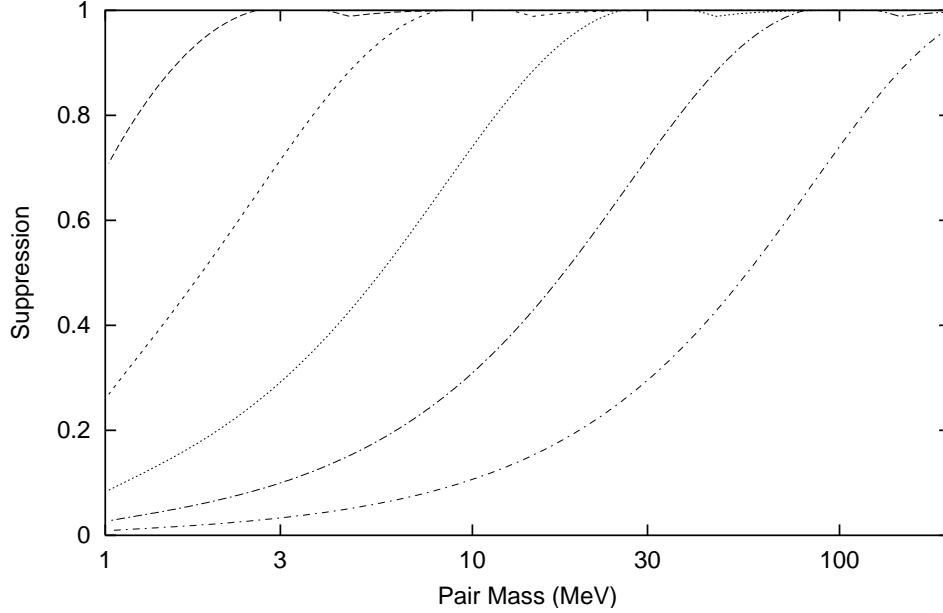


FIG. 6: The suppression factor $S = \sigma_{LPM}/\sigma_{BH}$ as a function of pair mass for photons with energies 44 TeV (top curve), 440 TeV, 4.4 PeV, 44 PeV and 440 PeV (bottom curve). The small dips below $S = 1$ around $M_p^2 \approx 8m^2k/E_{LPM}$ are side-ripples to the dips in Fig 5. These curves can be applied to other materials by scaling k by $E_{LPM}(\text{lead})/E_{LPM}$; the bottom curve also applies for 1.36 EeV photons in iron ($E_{LPM} = 13.6$ TeV).

With these details, Zakharov found a good fit to the SLAC E-146 data, except for the carbon.

V. N. Baier and V. M. Katkov made one of the few explicit calculations of pair production [39, 40]. The framework was similar to Migdal, but with a quasiclassical eikonal approximation for the scattering. This quasiclassical approach has been criticized as being inapplicable in the regime where it was used because the electron impact parameter cannot be treated classically [41]. However, Baier and Katkov argue that, when the angular momentum is large, their approach is acceptable [42]. The eikonal approach allowed them to include Coulomb corrections in the potential, an important factor in improving the accuracy of the calculations. They included a separate term in the potential to account for scattering from the atomic electrons. In the no-suppression limit, the authors obtain the fully-screened Bethe-Maximon Coulomb-corrected cross sections.

Baier and Katkov note that, for heavy elements, the Coulomb correction is larger than the uncertainties in the SLAC E-146 data [7]. The E-146 experimental analysis normalized

the Migdal calculations (without radiative corrections) to a radiation length that included Coulomb corrections, effectively multiplying the two effects together. This was the limit of the then-current technology. Although the results matched the data, this may not have been an optimal approach.

When the suppression is strong, Baier and Katkov give a polynomial expression for the total pair production cross section

$$\frac{\sigma}{\sigma_{BM}} \approx 4.28 \sqrt{\frac{E_{LPM}}{k}} \left[1 - 1.672 \sqrt{\frac{E_{LPM}}{k}} - 2.192 \frac{E_{LPM}}{k} + \frac{1}{4L_1} \left(\ln \frac{k}{4E_{LPM}} + 0.274 \right) \right] \quad (32)$$

where $L_1 = 183Z^{-1/3}e^{-f}$, with f from Eq. 8. Here, σ_{BM} is the Bethe-Maximon cross section [7] (apparently mis-labelled as Bethe-Heitler in Eq. 2.35 of Ref. [40]). The polynomial in Eq. 32 reduces the cross section at moderate photon energies. However, at large enough energies, the polynomial terms drop out, but the last correction term in Eq. 32 increases the cross section to 2-10% above the Migdal result.

Experimental Measurements of Suppression

Suppression of pair production can only be observed for photon energies $k > E_{LPM}$. Since $E_{LPM} > 1$ TeV, even for the densest materials, it has not been possible to study this suppression at accelerators. Some studies have used cosmic rays, but the statistics are limited by the high energy cosmic ray flux. The earliest studies considered low-energy electrons in photon induced showers. Fowler, Perkins and Pinau studied 47 electromagnetic showers with an energy above 1 TeV in an emulsion stack, measuring the distance between the initial conversion point and the first daughter pair downstream of the primary [43]. At high photon energies, the average distance rose, as expected for decreasing cross sections. The statistics were limited because few sufficiently energetic photons penetrate the atmosphere. To improve the statistics, some later experiments flew emulsion detectors in high-altitude balloons [44], where the flux of high-energy photons is higher. They achieved somewhat better statistics, but with qualitatively similar results.

One of the most precise studies was by Kasahara in 1985 [45]. He studied the development of electromagnetic showers with energies of order 100 TeV, in lead-emulsion chambers. At these energies, LPM suppression significantly increases the penetration depth of the showers. After removing the contamination from hadronic showers, Kasahara found that the shower

profiles were consistent with Migdals cross sections, but not the Bethe-Heitler formulae.

Because of the limited statistics possible in cosmic ray studies, the best studies of the LPM effect have used accelerators to study the suppression of bremsstrahlung. Bremsstrahlung can be studied with electron beams with energies $E \ll E_{LPM}$, as long as photons with energies $k < E^2/E_{LPM}$ are studied.

The first accelerator experiment used 40 GeV electrons generated from 70 GeV protons at the Serpukhov U-70 accelerator [46]. Bremsstrahlung photons from carbon, aluminum, lead and tungsten targets were detected in a sodium-iodide calorimeter. The electrons were bent away from the calorimeter with a magnet. The group studied photons with energies between 20 and 80 MeV. At higher photon energies, the LPM effect was unimportant, while at lower energies, the backgrounds were very high. Even in the signal region, there were significant backgrounds from bremsstrahlung in air and scintillation counters, and muon contamination in the beam. By taking ratios of their data (lead/aluminum and tungsten/carbon), they were able to estimate the degree of suppression. They found suppression larger than Migdal predicted, albeit with large errors.

A later experiment at the Stanford Linear Accelerator Center, SLAC Experiment E-146, made precise measurements of bremsstrahlung from 7 targets, from carbon to uranium, in beams of 8 and 25 GeV electrons [47, 48, 49]. They studied photons with energies between 200 keV and 500 MeV. The photons were detected in a position-sensitive segmented BGO calorimeter 50 meters away from the target. The small solid angle and position sensitivity helped reduce backgrounds, especially from synchrotron radiation. Data was taken at 2 different settings of calorimeter gain (i.e. photomultiplier tube high voltage) to maximize the dynamic range. The electron beam-line was kept entirely in vacuum to eliminate bremsstrahlung from air or target windows.

The group used a tertiary electron beam, but, because the primary beam was also electrons, beam contamination was small. The beam was usually run at an average of 1 electron per pulse, 120 pulses/second; events containing zero or multiple electrons were rejected during analysis.

The calorimeter was calibrated using cosmic rays and a 500 MeV electron beam. The group also used the downstream magnet for an electron spectrometer, measuring the electron energy loss. Because of the limited resolution for electron energy loss, this was useful only as a check.

Figure 7 shows the E-146 data for the aluminum targets. Targets with thicknesses of 3% and 6% of X_0 (3.12 mm and 5.3 mm) were used. Events containing a single electron were selected, and the photon energy spectrum measured. The photon energy is plotted in logarithmic width bins, with 25 bins per decade of energy. Then, the approximate Bethe-Heitler photon spectrum $dN/dk \approx 1/k$ transforms to $dN/d\ln(k)/X_0 \approx 0.13$ - a straight line. The probability for a single electron to undergo two independent interactions in the target tilts the spectra slightly. This was dealt with by using a Monte Carlo simulation.

The data shows significant suppression. For $k < 2 \times 10^{-4}E$, an additional suppression mechanism is required to explain the data. This second mechanism involves the produced photon, which also interacts with the medium, through forward Compton scattering. Classically, this is described via a dielectric constant $\epsilon \neq 1$.

The group has also studied thin targets, where $T < l_f$ for relevant photon energies. For thin targets, the radiation was above the Migdal calculation, and consistent with the calculations that treated the entire target as a single radiator.

More recently, an Aarhus-CERN-Florence-Free University, Amsterdam-Cape Town collaboration studied bremsstrahlung from 149-287 GeV electrons from iridium, tungsten and tantalum targets [50]. They used a CERN test beam. Figure 8 shows their tantalum target data plotted in a manner similar to the E-146 data. With the higher electron energies, they observed suppression up to $k/E \approx 0.16$, a significant fraction of the spectrum. The goal of this experiment was to directly observe the overall increase in radiation length as the radiation decreases. They observed roughly a 30% decrease in radiation at the highest electron energy, consistent with expectations from Migdals calculation.

The collaboration fitted their spectra to measure E_{LPM} for their targets [51]. For the densest target, iridium, their measured E_{LPM} averaged 1.97 ± 0.16 TeV, in quite good agreement with the theoretical prediction of 2.25 TeV. However, for the lighter targets, tantalum and copper, the measured E_{LPM} were considerably below the expected values - by 40% for copper. The reasons for the difference are not clear, but the collaboration suggests that possibly bremsstrahlung from atomic electrons could be unsuppressed. The experiment also uses data from a carbon target for a normalization spectrum; if the carbon spectra were somehow compromised, this data could affect their measured E_{LPM} . It may be worth noting that the E-146 carbon-target data is poorly described by calculations based on Migdals work.

PAIR PRODUCTION IN CONSTANT FIELDS AND CRYSTALS

Over 50 years ago, H. Robl noted that for very high energy photons, matter is not necessary for pair production: even static electromagnetic fields suffice [52]. This is analogous to synchrotron radiation. The photon conversion depends on the parameter

$$\chi = \frac{kB_{\perp}}{2mB_c} \quad (33)$$

where B_{\perp} is the magnetic field perpendicular to the photon direction and $B_c = m^2/eh = 4.4 \times 10^{13}$ Gauss is the critical field. The probability of photon survival for a distance d is

$$P(d) = \exp(-ad) \quad (34)$$

where [53]

$$a = \frac{0.16\alpha m}{\lambda_e k} K_{1/3}^2(2/3\chi) \quad (35)$$

and $K_{1/3}(x)$ is a modified Bessel function and $\lambda_e = 386$ fm is the Compton wavelength of the electron. This equation is for the constant field approximation, and may fail for rapidly varying fields. Figure 9 shows the attenuation coefficient a for photons of different energies. The absorption is small for $\chi \ll 1$, or $k < 2mB_c/B_{\perp}$. In this limit $a = 0.46 \exp(-4/3\chi)$. The absorption rises sharply as a function of k for $\chi > 1$, reaching a peak for $k = 12mB_c/B_{\perp}$. At this maximum, $a \approx 0.1(\alpha/\lambda_e)B_{\perp}/B_c$. As χ continues to rise, the attenuation coefficient drops slowly; for $\chi > 1000$, $a \approx 0.6\chi^{-1/3} \approx B_{\perp}^{2/3}k^{-1/3}$. The attenuation increases with increasing B_{\perp} , but, for fixed B_{\perp} , drops slowly as k rises.

There are some minor discrepancies between various studies. Erber [53] uses a dimensionless auxiliary function $T(\Upsilon)$ to calculate α . His Eq. 3.3d, defines $T(\Upsilon)$, with numerically matching small and large Υ limits in Eq. 3.3c. However, Fig. 9 and Table VI of Ref. [53] give $T(\Upsilon)$ are half as large as the equations; the equations appear to be correct. Ref. [54] plots photon attenuation following the equations in Erbers review.

The momentum transfer to the field required for pair production is the same as for an atomic target, Eq 3. Additional terms are required to account for the magnetic bending which, like multiple scattering, reduces the electron and positron longitudinal velocity. The field bends electrons smoothly, with

$$\theta_B = \frac{eB_{\perp}l_f}{E}, \quad (36)$$

in contrast to the $\theta \approx \sqrt{l_f}$ found for multiple scattering. Including the magnetic bending for the electron (θ_{B-}) and positron (θ_{B+}), the longitudinal momentum transfer is

$$q_{\parallel} = \frac{M_p^2}{2k} + \frac{E\theta_{B-}^2}{2} + \frac{(k-E)\theta_{B+}^2}{2} = \frac{M_p^2}{2k} + \frac{e^2 B_{\perp}^2 l_f^2 k}{2E(k-E)} \quad (37)$$

This leads to a quartic equation for l_f . At low photon energies, magnetic bending is small and l_f rises linearly with k . It reaches a maximum, and then decreases. For $\chi \gg 1$,

$$l_f = \left(\frac{\hbar E(k-E)}{e^2 B_{\perp}^2 k} \right)^{1/3} = \left(\frac{\hbar k m^2}{e^2 B_{\perp}^2 M_p^2} \right)^{1/3}, \quad (38)$$

so $l_f \approx k^{1/3}/B_{\perp}^{2/3}$ - the same scaling found from the more detailed calculations.

Since B_c is so large, this process is only important for photons with quite high energies. In fact, conversion in an external magnetic field has not been observed. However, it does have important astrophysical applications. One example involves very high energy cosmic rays. Very high energy photons may pair convert in the earth's magnetic field [54, 55, 56]. For a $k = 10^{20}$ eV photon perpendicular to the earth's field, the attenuation length is about 100 km. The earth's magnetic field extends to altitudes of 1000's of kilometers, far above the atmosphere where lower energy showers originate. The produced electrons interact with the earth's magnetic field and emit synchrotron radiation. The combination of pair production in the field and synchrotron radiation leads to an electromagnetic shower, even in the absence of matter. The field-induced shower largely stops developing when the average particle energy drops so that $\chi \ll 1$ ($\approx 10^{19.5}$ eV). The produced particles propagate downward until they reach the atmosphere, where the shower develops conventionally. The initial high-altitude reactions gives these showers a head-start. This early development is helpful in differentiating photon initiate showers from proton initiated showers. Only a handful of showers with energies above 10^{20} eV have been observed, but the primary particles cannot all be photons [28].

Pair conversion can also occur in the strong magnetic fields that surround many astrophysical objects. For example, many neutron stars support surface magnetic fields around 10^{12} G. In these fields pair conversion occurs quickly for $k > 50$ MeV.

Although pair conversion from an external magnetic field has not been seen in the laboratory, a fairly close analog has been studied: pair conversion in crystals. When a photon traverses a crystal parallel to one of the axes, the magnetic fields of the individual atoms add together to act as a single, extremely strong field. The effective fields are largest when

the photon direction is well aligned with a crystal axis, within a characteristic angle given by the atomic lattice spacing divided by the formation length. For 100 GeV photons, this angle is a few mrad. Often, the target is mounted in a goniometer which allowed precise adjustments of the crystal orientation. Pair conversion is studied as the crystal orientation is varied; when the axis is properly aligned, pair production is enhanced [60].

Two factors affect the enhancement. Impurities and other lattice defects lead to uneven atom spacings which reduce the coherence; high quality crystals are required. The quality requirement limits the choice of target material. At the highest photon energies, variations in atomic spacing due to lattice vibrations limit the coherence. Sometimes, crystals are cooled to reduce these vibrations. The second factor is the divergence (angular size) of the photon beam. In a beam with a large divergence, many photons will not be within the characteristic angle of the crystal axis.

The simplest manifestation of the strong coherent fields is channelling; charged particles in crystals may be strongly deflected. Channeling studies show that the effective fields can reach 25 Megagauss in silicon crystals [57]. Crystal channeling can in some cases supplant conventional accelerator magnets, particularly for beam extraction [58].

With the increased bending, production of bremsstrahlung photons is also greatly enhanced. This technique is mature enough that plans are advanced to use coherent bremsstrahlung in a diamond crystal to generate high-energy polarized photon beams for a series of experiments [59].

The fields can also cause photon conversions. At CERN, pair conversion in germanium, tungsten and iridium crystals has been studied with photons with energies up to 150 GeV. The pair production cross section was enhanced over the isolated atom Bethe-Heitler prediction; the enhancement grew linearly with energy, reaching a factor of 7 for $k = 150$ GeV [61]. The total and differential (with respect to E/k) cross sections agreed with the predictions for coherent enhancement.

When a magnetic field also contains matter, both fields must be considered together. The effects of the nuclei and the fields must be combined to find the conversion probability. This is a complex calculation. Here we examine one limit, the reduction in pair conversion on a target due to the motion caused by a moderate ($\chi < 1$) magnetic field. Here, the magnetic field plays a similar role to multiple scattering. When the magnetic bending terms in Eq. 37 dominate, the magnetic field suppresses the bremsstrahlung. The suppression equation

is quartic, and, in the limit of strong suppression, the cross section is [5]

$$\sigma = \sigma_{BH} \left(\frac{kE_B}{E(k-E)} \right)^{2/3} \quad (39)$$

where

$$E_B = \frac{mB_c}{B_\perp} \quad (40)$$

plays a similar role to E_{LPM} . This approach only applies for very high energy photons in relatively low-density matter. At high densities, LPM suppression dominates. When $\chi > 1$, pair conversion in the magnetic field is important. A parallel analysis finds a similar suppression for bremsstrahlung. The bremsstrahlung calculation is supported by detailed calculation using kinetic equations [62].

PAIR PRODUCTION AT PARTICLE COLLIDERS

Pair production also occurs at particle colliders. The colliding particles each emit a photon; the two photons collide to form an e^+e^- or other lepton pair. Lepton pair production at e^+e^- colliders has been studied intensely over the past 30 years. These studies have been used for a variety of tests of QED [63]. The reactions have also been studied as backgrounds to other interesting processes, especially those that are beyond the standard model. They are also used to measure the internal (electromagnetic) structure of the photon [64].

Although these processes follow the same diagrams as pair production, Fig. 1, there are some significant differences from the fixed target regime. The reaction $e^+e^- \rightarrow e^+e^-e^+e^-$, studied at e^+e^- colliders, involves many more diagrams than appear in Fig. 1. Second, the photons are virtual. For e^+e^- colliders, and ep colliders, the virtuality (effective mass) is large, while in proton and ion colliders it is smaller. This review will focus on photoproduction with almost-real photons (those with small virtuality) at ep , $pp/\bar{p}p$ and heavy ion colliders. Finally, the symmetric initial state leads to some interesting effects. There is a vast literature on photoproduction at colliders; here we only consider a few selected examples to illustrate the similarities and differences with fixed target reactions.

Muon and electron pair production, $ep \rightarrow epe^+e^-$ and $ep \rightarrow ep\mu^+\mu^-$ were studied by the H1 collaboration at the HERA ep collider [65]. They observed lepton pairs with masses up to 80 GeV, where electroweak corrections to QED are significant. The study was done to

search for physics beyond the standard model, but the collaboration found good agreement with the standard model.

In colliders, the ions are fully stripped of electrons. There is no screening, and, as the beam energy rises, photoproduction occurs at larger and larger impact parameters. Consequently, the cross section continues to rise with energy indefinitely. For example, in gold on gold collisions at a center of mass energy of 200 GeV per nucleon at Brookhaven's Relativistic Heavy Ion Collider, the cross section is expected to be 33,000 barns, rising to 200,000 barns in 5.5 TeV per nucleon lead on lead collisions at CERN's Large Hadron Collider [12]. Pair production can occur at ion-ion separations up to several μm .

Because $Z\alpha \approx 0.6$, higher order corrections to the cross section could be large, and pair production may probe non-perturbative strong-field QED. This possibility encouraged many theoretical efforts. One approach extended the Bethe-Maximon approach to collisions of heavy ions. The effect of the Coulomb potentials of both ions was to reduce the cross section by 25% at RHIC and 14% at the LHC [66].

Tony Baltz made an all-orders calculation of pair production in ultra-relativistic heavy ion collisions. He found an exact solution to the time-dependent Dirac equation [67]. In an appropriate gauge, the Coulomb potential from an ultra-relativistic particle simplifies into a simple two-dimensional potential, and pair production can be calculated exactly. Surprisingly, his results matched the lowest order perturbative result [67], without any Coulomb corrections. However, a later, more careful calculation found results that included the Coulomb corrections [68]. The theoretical issues are discussed elsewhere in this volume, so they will not be considered further here.

In most existing data on e^+e^- production in ion collisions, at least one of the ions is light (typically sulfur). Experiment NA-45 at the CERN SPS studied 200 GeV per nucleon bare sulfur ions hitting a platinum target and found cross sections consistent with the lowest order perturbative result [69]. The measured cross section in a restricted kinematic region is $0.99_{-0.28}^{+0.33}$ of that expected from lowest order QED. Here, the errors are combined in quadrature. This result could be used to put limits on some models of radiative corrections. Other SPS studies found similar results, with general agreement to lowest order calculations [70, 71].

At ion colliders, the charges are large enough that multiple interactions between a single ion pair are very possible. For example, two pairs may be created by a single ion-ion reaction

[72]. Multiple pairs have not been studied yet. However, the STAR collaboration has studied e^+e^- pair production accompanied by mutual Coulomb dissociation of the two nuclei [73, 74]. The mutual Coulomb dissociation criteria selects collisions where the impact parameter is less than about 30 fm, considerably smaller than for unselected pair production. The reduction in impact parameter leads to stronger colliding fields, and therefore to increased higher order corrections. Despite this, the collaboration found that their results were well described by lowest order QED. They did find that it was necessary to include the photon virtuality in the calculation to explain the p_T spectrum of the pair.

Multiple interactions are most common at small impact parameters, where the field densities are strongest. For this reason, they are a good place to search for higher order effects. Despite this, the STAR data are consistent with lowest order QED. Because of the restricted impact parameter range, this data cannot be directly compared with existing studies of radiative corrections [74].

The absence of atomic electrons allows some new reactions, such as pair production with capture, where an electron is produced bound to one of the participating nuclei. This reaction has a number of notable applications, most notably the first production of antihydrogen. Antihydrogen is produced when positrons were produced via pair production, bound to antiprotons [75]. At heavy ion colliders, the cross section for electron capture is sizable, of the order of 100-200 barns at RHIC and the LHC [76]. The single-electron atoms are lost from the colliding beams, reducing the luminosity, and giving pair production some importance for accelerator design.

CONCLUSIONS

Pair production at high energies covers a varied palette of physics. High mass pairs have been a sensitive test of QED, and pair production at e^+e^- and ep colliders continues to be a laboratory to search for new physics. These colliders allow the highest energy tests of QED.

Lower mass pairs have long formation lengths. These reactions are distributed over many atoms, and probe bulk characteristics of the material. When the photon energy is large enough, pair production is suppressed below the Bethe-Heitler cross section, and many ‘obvious’ scaling laws fail. At very high photon energies, the pair production cross section may be smaller than the photonuclear cross section, and photonic showers will look like

hadronic showers.

Pairs may also be produced in strong magnetic fields. This has significant implications in astrophysics. These strong magnetic fields also appear in crystals when the photon is aligned with one of the crystal axes. These aligned photons may coherently convert to e^+e^- pairs.

I would like to thank Ulrik Uggerhøj for permission to reprint Fig. 8 and for useful discussions. Kai Hencken, Gerhard Baur, Roman Lee and Hristofor Vankov all provided useful suggestions. This work was supported by the U.Sy. Department of Energy under Contract No. DE-AC-03076SF00098.

-
- [1] C. D. Anderson, Phys. Rev. **41**, 405 (1932); **43**, 491 (1933); **44**, 406 (1933).
 - [2] H. A. Bethe and W. Heitler, Proc. R. Soc. London, Ser A **146**, 83 (1934).
 - [3] B. Rossi and K. Greisen, Rev. Mod. Phys. **13**, 240 (1941).
 - [4] K. Hagiwara *et al.*, Phys. Rev. **D66**, 010001 (2002).
 - [5] S. Klein, Rev. Mod. Phys. **71**, 1501 (1999); S. Klein, hep-ex/0112018.
 - [6] A. I. Akhiezer and N. F. Shulga, “High Energy Electrodynamics in Matter,” Gordon and Breach, New York, 1996.
 - [7] V. N. Baier and V. M. Katkov, hep-ph/0309211.
 - [8] M. L. Ter-Mikaelian, *High Energy Electromagnetic Processes in Condensed Media*, (Wiley, New York), 1972.
 - [9] G. D. Palazzi, Rev. Mod. Phys. **40**, 611 (1968).
 - [10] A. H. Sørensen, Nucl. Instrum. & Meth. **B119**, 1 (1996).
 - [11] V. N. Baier, V. M. Katkov and V. M. Strakhovenko, Sov. Phys. Usp **32**, 972 (1989).
 - [12] G. Baur *et al.*, Phys. Rept. **364**, 359 (2002).
 - [13] Y. S. Tsai, Rev. Mod. Phys. **46**, 815 (1974).
 - [14] H. A. Bethe and L. C. Maximon, Phys. Rev. **93**, 768 (1954).
 - [15] H. Davies, H. A. Bethe and L. C. Maximon, Phys. Rev. **93**, 788 (1954).
 - [16] R. N. Lee, A. I. Milstein and V. M. Strakhovenko, hep-ph/0310108.
 - [17] S. J. Brodsky and J. R. Gillespie, Phys. Rev. **173**, 1011 (1968).
 - [18] J. G. Astbury *et al.*, Phys. Lett. **25B**, 565 (1967).

- [19] J. Eickmeyer *et al.*, Phys. Rev. **D21**, 3001 (1980).
- [20] R. F. Cahalan and K. O. Mikaelian, Phys. Rev. **D10**, 3769 (1974).
- [21] L. D. Landau and I. J. Pomeranchuk, Dokl. Akad. Nauk. SSR **92**, 535 (1953).
- [22] L. D. Landau and I. J. Pomeranchuk, Dokl. Akad. Nauk. SSR **92**, 735 (1953).
- [23] J. D. Jackson, *Classical Electrodynamics*, (Wiley, New York), 1995.
- [24] E. L. Feinberg and I. Pomeranchuk, Nuovo Cim. Suppl. A1, series X **III**, 652 (1956).
- [25] R. Engel, J. Ranft and S. Roesler, Phys. Rev. **D55**, 6957 (1997).
- [26] J. P. Ralston, S. Razzaque and P. Jain, astro-ph/0209455.
- [27] V. M. Galitsky and I. I. Gurevich, Nuovo Cimento **32**, 396 (1964).
- [28] M. Nagano and A. A. Watson, Rev. Mod. Phys. **72**, 689 (2000).
- [29] S. Klein, astro-ph/9712198.
- [30] F. Halzen, astro-ph/0311004.
- [31] N. F. Shulga and S. P. Fomin, JETP Lett. **63**, 873 (1996).
- [32] V. N. Baier and V. M. Katkov, Phys. Lett. **A252**, 263 (1999).
- [33] F. F. Ternovskii, Sov. Phys. JETP **12**, 123 (1961).
- [34] A. B. Migdal, Phys. Rev. **103**, 1811 (1956).
- [35] T. Stanev *et al.*, Phys. Rev. **D25**, 1291 (1982).
- [36] R. Blankenbecler and S. D. Drell, Phys. Rev. **D53**, 6265 (1996).
- [37] B. G. Zakharov, JETP Lett. **63**, 952 (1996); JETP Lett. **64**, 781 (1996).
- [38] B. G. Zakharov, Phys. At. Nucl. **61**, 838 (1998); B. G. Zakharov, Phys. At. Nucl. **62**, 1008 (1999).
- [39] V. N. Baier and V. M. Katkov, Phys. Rev. **D57**, 3146 (1998).
- [40] V. N. Baier and V. M. Katkov, Phys. Rev. **D62**, 036008 (2000).
- [41] B. G. Zakharov, hep-ph/9908449.
- [42] V. N. Baier and V. M. Katkov, hep-ph/9910202.
- [43] P. H. Fowler, D. H. Perkins and K. Pinkau, Philos. Mag. **4**, 1030 (1959).
- [44] E. Lohrmann, Phys. Rev. **122**, 1908 (1961); S. C. Strausz *et al.*, in *Proc. 22nd Intl. Cosmic Ray Conf.*, Dublin, Ireland, 1991, vol 4, pg. 233.
- [45] K. Kasahara, Phys. Rev. **D31**, 2737 (1985).
- [46] A. Varfolomeev *et al.*, Sov. Phys. JETP **42**, 218 (1976).
- [47] P. Anthony *et al.*, Phys. Rev. Lett. **75**, 1949 (1995).

- [48] P. Anthony *et al.*, Phys. Rev. Lett. **76**, 3550 (1996).
- [49] P. Anthony *et al.*, Phys. Rev. **D56**, 1373 (1997).
- [50] H. D. Hansen *et al.* Phys. Rev. Lett. **91**, 014801 (2003).
- [51] H. D. Hanse *et al.*, to appear in Phys. Rev. **D**, 2004.
- [52] H. Robl, Acta Phys. Austriaca **6**, 105 (1952).
- [53] T. Erber, Rev. Mod. Phys. **38**, 626 (1966).
- [54] H. P. Vankov, N. Inoue and K. Shinozaki, Phys. Rev. **D67**, 043002 (2003).
- [55] B. McBreen and C. J. Lambert, Phys. Rev. **D24**, 2536 (1981).
- [56] T. Stanev and H. P. Vankov, Phys. Rev. **D55**, 1365 (1997).
- [57] A. Baurichter *et al.*, Nucl. Instrum. & Meth. **B164**, 27 (2000).
- [58] V. Guidi *et al.*, preprint physics/0306126.
- [59] P. Bosted, Int. J. Mod. Phys. **A18**, 1169 (2003).
- [60] R. Moore *et al.*, Nucl. Instrum. & Meth. **B119**, 149 (1996).
- [61] K. Kirsebom *et al.*, Nucl. Instrum. & Meth. **B135**, 143 (1998).
- [62] V. N. Baier, V. M. Katkov and V. M. Strakhovenko, Sov. Phys. JETP **67**, 70 (1988).
- [63] V. M. Budnev, I. F. Ginzburg, G. V. Meledin and V. G. Serbo, Phys. Rept. **15**, 181 (1974)
- [64] P. Abreu *et al.*, Eur. Phys. J. **C19**, 15 (2001); D. Buskulic *et al.*, Phys. Lett. **B388**, 419 (1996); H. Hayashii *et al.*, Phys. Lett. **B279**, 422 (1992); M. Petradza *et al.*, Phys. Rev. **D42**, 2180 (1990).
- [65] B. Leissner, Dissertation, Technischen Hochschule Aachen, Oct. 2002.
- [66] D. Yu Ivanov, A. Schiller and V. Serbo, Phys. Lett. **B454**, 155 (1999).
- [67] A. J. Baltz, Phys. Rev. Lett. **78**, 1231 (1997).
- [68] R. N. Lee and A. I. Milstein, Phys. Rev. **A61**, 032103 (2000).
- [69] R. Baur *et al.*, Phys. Lett. **B332**, 471 (1994).
- [70] C. R. Vane *et al.*, Phys. Rev. **A50**, 2313 (1994); C. R. Vane *et al.*, Phys. Rev. Lett. **69**, 1911 (1992).
- [71] J. H. Derrickson *et al.*, Phys. Rev. **A51**, 1253 (1995).
- [72] A. Alscher, K. Hencken, D. Trautmann and G. Baur, Phys. Rev. **A55**, 396 (1996).
- [73] V. Morozov, PhD dissertation, UC Berkeley, 2003.
- [74] J. Adams *et al.* (STAR Collaboration), nucl-ex/0404012; S. Klein for the STAR Collaboration, nucl-ex/0310020.

- [75] G. Baur *et al.*, Phys. Lett. **B368**, 251 (1996); G. Blandford *et al.*, Phys. Rev. Lett. **80**, 3037 (1998).
- [76] G. Baur, K. Hencken and D. Trautmann, J. Phys. **G24**, 1657 (1998).

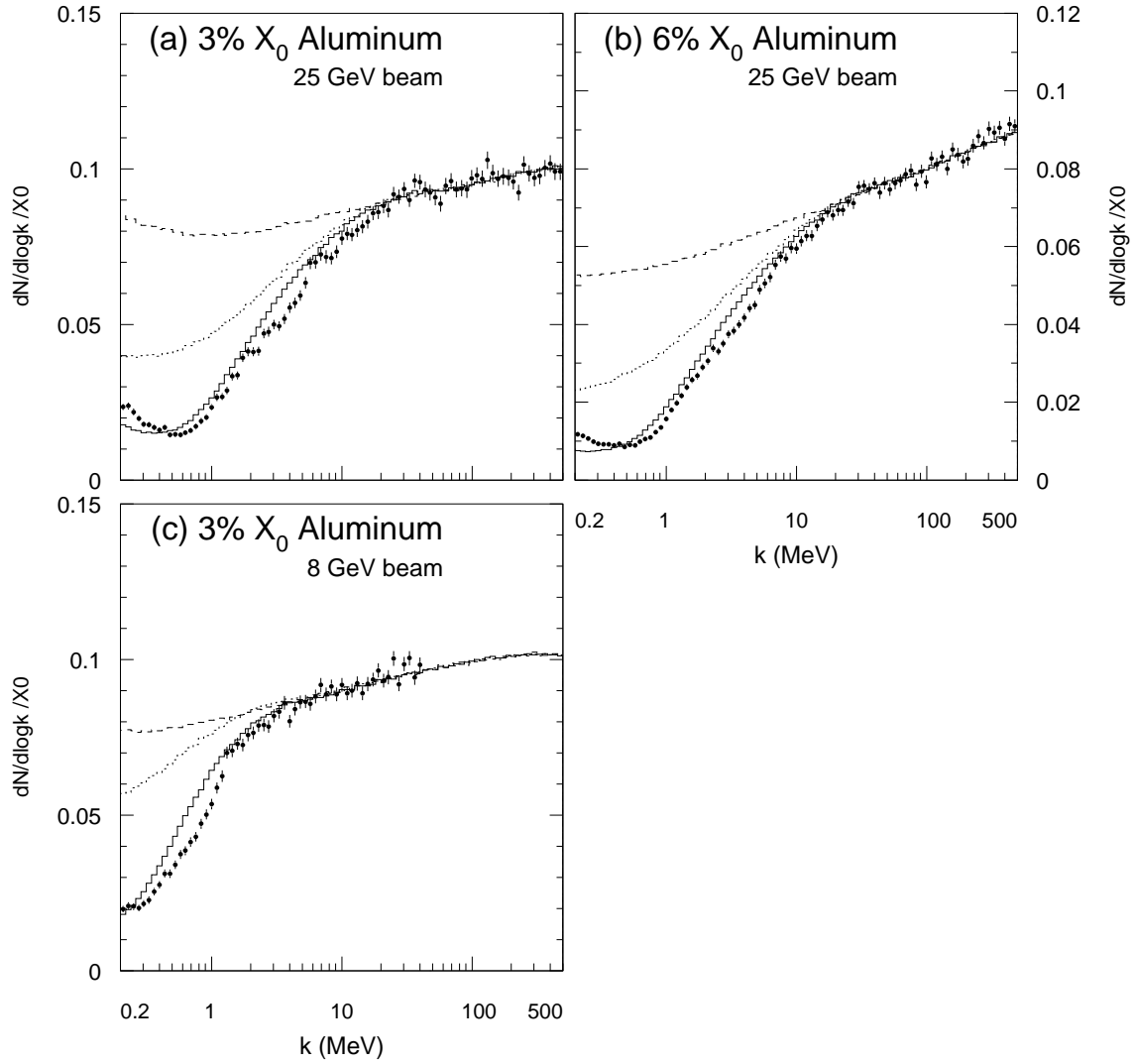


FIG. 7: SLAC Experiment E-146 data (points) compared with Monte Carlo predictions using the Bethe-Heitler (dashed line), LPM suppression (dot-dashed line) and with LPM and dielectric suppression (solid line). The simulations include transition radiation. Adapted from Ref. [49].

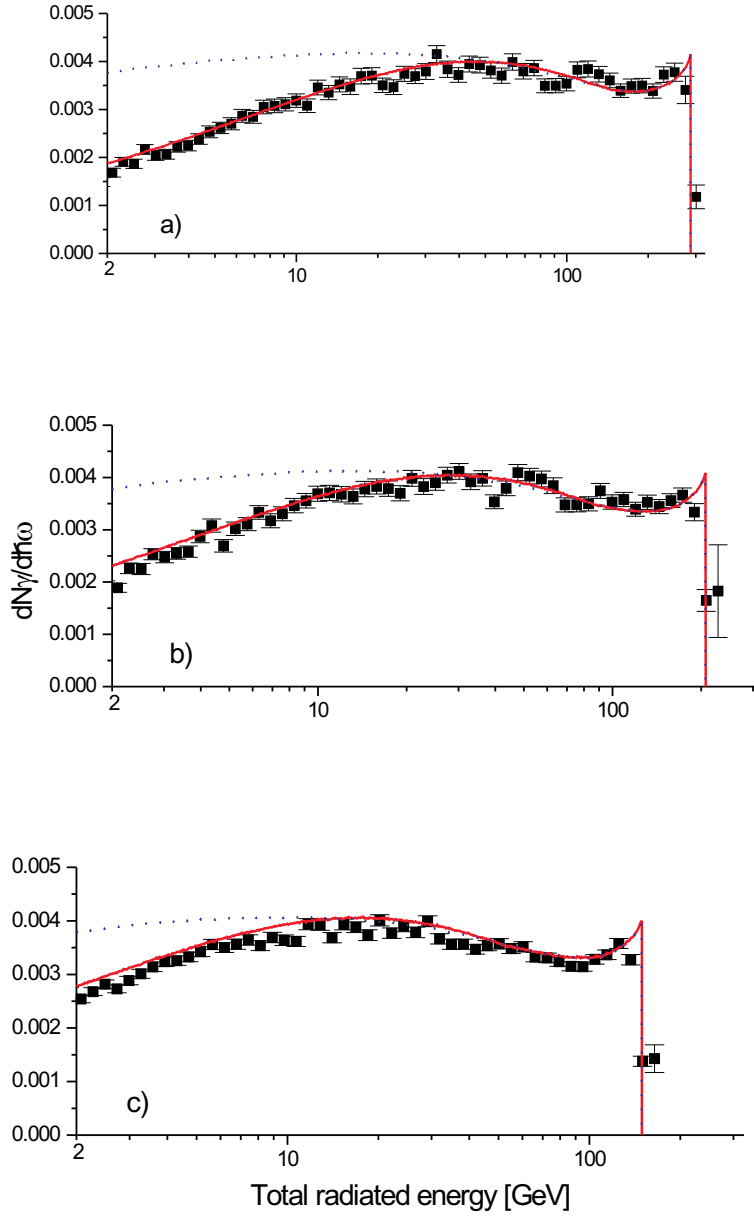


FIG. 8: Bremsstrahlung spectrum from (a) 287 GeV, (b) 207 GeV and (c) 149 GeV electrons striking a 0.128 mm thick iridium target. The photon energy scale is logarithmic, with 25 bins per decade if energy. The dotted line is a simulation using the Bethe-Heitler spectrum, while the solid line includes LPM suppression. From Ref. [50].

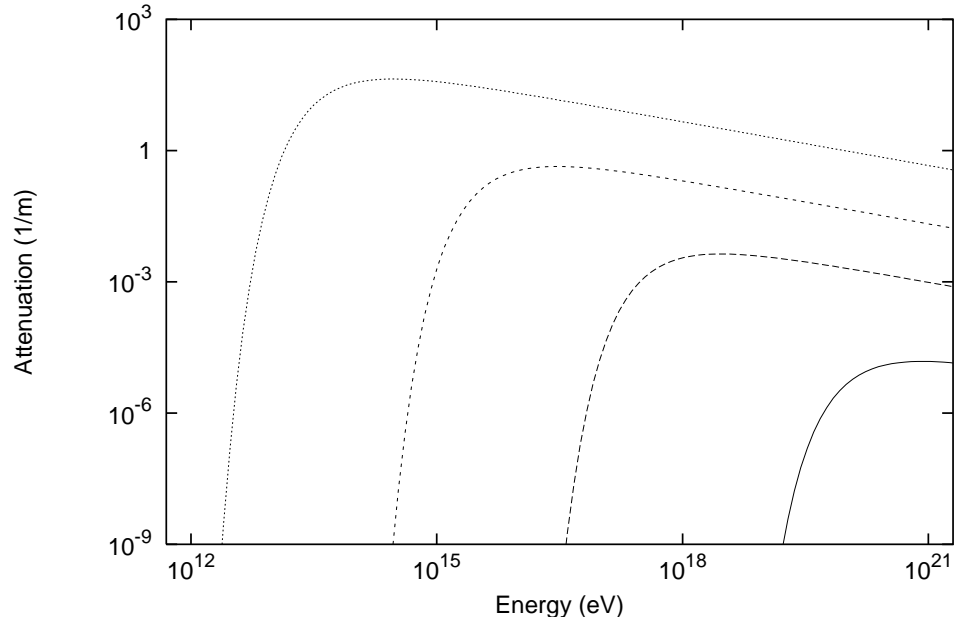


FIG. 9: Attenuation coefficient (inverse attenuation length) for photons in a magnetic field with perpendicular components of 0.35 Gauss (the Earth's average field - solid line), 100 Gauss (short dashes), 10^4 Gauss (long dashes) and 10^6 Gauss (dotted line).